

Improved grid voltage sensorless control strategy for railway power conditioners

ISSN 1755-4535

Received on 24th August 2014

Revised on 29th May 2015

Accepted on 4th July 2015

doi: 10.1049/iet-pel.2014.0673

www.ietdl.org

Amir Masoud Bozorgi¹ ✉, Majid Sanatkar Chayjani², Reza Mohammad Nejad³,
 Mohammad Monfared²

¹Department of Electrical Engineering, Khorasan Institute of Higher Education, Mashhad, Iran

²Department of Electrical Engineering, PELab, Ferdowsi University of Mashhad, Mashhad, Iran

³Department of Management, Ferdowsi University of Mashhad, Mashhad, Iran

✉ E-mail: amir.m.bozorgi@khorasan.ac.ir

Abstract: Rapid development of high-speed trains confronts the power grid with serious power quality problems. In this study, to compensate power quality, an improved grid voltage sensorless control method for the railway power conditioner (RPC) is proposed. The proposed control strategy utilises a moving average filter to better detect the compensating currents and a proportional-resonant controller to control the compensating currents. Moreover, a sensorless virtual flux method based on second order low-pass filters is presented to replace the AC voltage sensors. Using the proposed strategy, the dynamic and steady-state characteristic of the RPC is significantly enhanced. Through simulation tests, the effectiveness of the proposed methods is confirmed.

Nomenclature

V	RMS value of grid side phase voltages
K_T	turns ratio of traction transformer
K_S	turns ratio of step-down transformers
i_{La}, i_{Lb}	current of loads a and b
I_{La}, I_{Lb}	RMS value of active current of loads a and b
I_{La}, I_{Lb}	RMS value of reactive current of loads a and b
I_{Lah}, I_{Lbh}	RMS value of h th order harmonic current of loads a and b
$\varphi_{ah}, \varphi_{bh}$	phase angle of h th order harmonic current of loads a and b
L_a, L_b	filter inductance of converters a and b
R_a, R_b	filter resistance of converters a and b
ψ_{ac}, ψ_{bc}	virtual flux at secondary side of step-down transformers a and b
v_{ref-a}, v_{ref-b}	reference voltage of converters a and b
V_{DC}	voltage of DC-link capacitor

1 Introduction

The distinctive features of high-speed trains lead to rapid development of electrified railways around the world. In spite of many practical successes of electric railway systems, using two independent single-phases for the traction supply system and also the frequent and non-linear nature of the load currents entail some power quality issues [1–3]. Considerable negative-sequence and harmonic components of currents generated from electric locomotives can give rise to adverse effect on safe and economic operation of the electric power grid [4–6].

To effectively alleviate the impact of electrified railways on the power quality of the utility grid, various techniques have been proposed [7–14]. Although some methods can be helpful to improve the power quality to some extent, they cannot be considered as a comprehensive approach for power quality compensation. Sequence rotation, reasonable locomotive operation modes or using balanced transformers and so on can attenuate the effects of negative-sequence contents (NSCs) on the grid [7, 8]. Nevertheless, these methods are not flexible and the system cannot maintain its balanced condition under variation of traction loads. Furthermore, the compensation of

reactive power and harmonics remain unsolved. Passive power quality compensators, for example, reactive power compensation capacitors and passive filters, are only able to eliminate some specific harmonics or a limited spectrum of harmonics [9].

In comparison with passive compensators, active compensators can be a superior solution. Static var compensators (SVCs) can be used to compensate reactive currents and NSCs; however, they must be connected to the high-voltage side of the system, and so, the rating and cost are increased [10, 11]. Moreover, SVC may degrade the power factor of the traction system if it is adopted for negative sequence compensation [12]. The active power quality compensator (APQC), proposed in [13], can compensate all power quality factors, such as NSCs and harmonic and reactive currents. Scott transformers used in APQC transforms two orthogonal and balanced single-phase voltages to balanced three-phase voltages for feeding a three-phase converter. Due to the Scott transformer features, using an unbalanced transformer in traction substations can upset the NSC compensation goal. As a result, a useful unbalanced topology such as three-phase V/V traction will not be helpful in this compensation method. Among different compensation approaches, railway static power conditioners (RPCs) have attracted much attention. A RPC is composed of two converters connected back to back through a common DC capacitor and can compensate NSCs and harmonic and reactive currents for traction systems. The RPC implementations with various transformer topologies have been studied so far, but due to a simple and low cost structure of three-phase V/V transformers, this topology is adopted in current study.

On the other hand, different detection as well as compensation methods are available for RPCs [15, 16]. In [16], Luo *et al.* elaborated a simple and effective strategy for realisation of detection and control of RPC. In this paper, an improved control strategy based on this method is proposed aiming to ameliorate the control performance. In this improved control strategy, a moving average filter (MAF) is incorporated to enhance the detection of fundamental active power currents and the dynamic performance of control loop. Furthermore, to attain the stable control of DC-link voltage, a proportional integral (PI) controller and a low pass filter are added to the outer voltage loop.

To realise current control of RPC, the hysteresis comparator was used in [16]. In spite of high dynamic of hysteresis control

method, variable switching frequency can be regarded as its main drawback. To deal with this problem, a PWM modulator with a current controller can be used. In [15], a recursive PI controller based on fuzzy rules was proposed to track the reference signals. This is a time consuming method and can increase the computational burden. In this paper, a proportional-resonant (PR) controller is designed and utilised in the current control loop, which can eliminate the steady state current tracking error.

Regarding the grid-connected voltage source converters, voltage sensorless strategies arouse considerable interest for cost reduction and increased reliability. A large variety of strategies has been reported for voltage sensorless operation of grid-connected converters [17–19], which can be adopted for RPCs. In Section 4, a virtual flux (VF) method based on second order low-pass filters (LPFs) is proposed for estimation of grid side voltages. Finally, through simulation tests, the validation of the proposed methods is confirmed.

2 Compensation strategy of RPC using three-phase V/V transformers

2.1 Traction system structure

The RPC structure in a system with a three-phase V/V traction transformer is depicted in Fig. 1. Because of simple structure and high power rating utilisation of three-phase V/V transformers, they are widely employed in high-speed railway traction systems. The 220-kV high voltage of grid utility is stepped down into two 27.5-kV single-phase voltages via a V/V transformer. The RPC is composed of two single phase voltage source converters connected in such a way that they share a common DC capacitor. These converters are connected to the feeder sections through two step-down transformers and the output inductive filters. Compensation can be fulfilled when both converters are used as current sources to transfer certain current from one power supply arm to the other based on control strategy.

2.2 Compensation principle

Assume the phase voltage vectors of the power grid are

$$\begin{cases} \vec{v}_A = V e^{j0} \\ \vec{v}_B = V e^{-j(2\pi/3)} \\ \vec{v}_C = V e^{j(2\pi/3)} \end{cases} \quad (1)$$

Vector diagram of the power grid voltages is shown in Fig. 2a. In this condition, the secondary voltages of three-phase V/V transformer will be

$$\begin{cases} \vec{v}_{ac} = \frac{\sqrt{3}V}{K_T} e^{-j(\pi/6)} \\ \vec{v}_{bc} = \frac{\sqrt{3}V}{K_T} e^{-j(\pi/2)} \end{cases} \quad (2)$$

Fig. 2b illustrates the vector diagram of the secondary side voltage vectors.

Assuming a four-quadrant PWM converter is employed for the train, the power factor of the loads is almost unity; therefore, the load currents of the right- and left-hand side sections are in phase with v_{ac} and v_{bc} , respectively. Furthermore, the currents are considered purely sinusoidal for the sake of simplicity of current analysis. Hence, the currents of feeder sections in absence of RPC can be expressed as

$$\begin{cases} \vec{i}_a = I_{Laa} e^{-j(\pi/6)} \\ \vec{i}_b = I_{Lba} e^{-j(\pi/2)} \end{cases} \quad (3)$$

It is assumed that two sections are loaded unequally. Hence, under uncompensated situation, the three-phase currents of the power

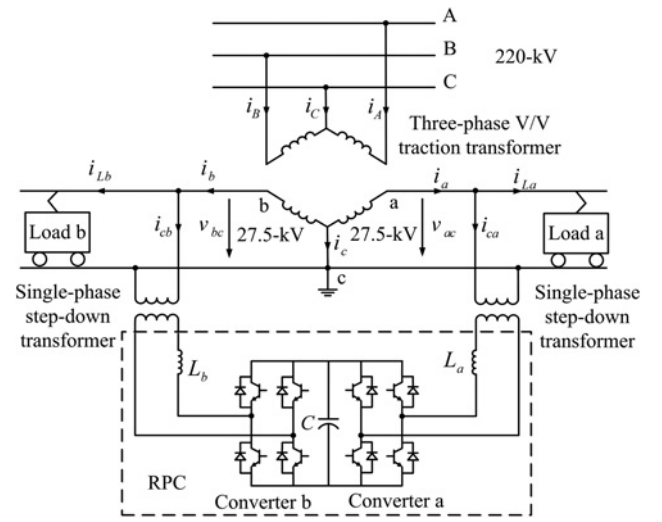


Fig. 1 RPC structure in a system with a three-phase V/V traction transformer

grid can be deduced as

$$\begin{cases} \vec{i}_A = \frac{I_{Laa}}{K_T} e^{-j(\pi/6)} \\ \vec{i}_B = \frac{I_{Lba}}{K_T} e^{-j(\pi/2)} \\ \vec{i}_C = -\left(\frac{I_{Laa}}{K_T} e^{-j(\pi/6)} + \frac{I_{Lba}}{K_T} e^{-j(\pi/2)} \right) \end{cases} \quad (4)$$

Having examined (4), one can see that there is a significant negative sequence in the grid current. To have tangible sense of the unbalancing amount, the current unbalance factor (CUF) can be defined as

$$\text{CUF} = \frac{|I_-|}{|I_+|} \times 100\% = \frac{\sqrt{I_{Laa}^2 + I_{Lba}^2 - I_{Laa}I_{Lba}}}{I_{Laa} + I_{Lba}} \times 100\% \quad (5)$$

In this equation, I_- and I_+ are negative and positive sequence currents, respectively. Given (5), at the best situation, when two sections have the same load, CUF becomes 50%, and whenever only one section is loaded, CUF has its maximum amount of 100%. Therefore, a significant amount of negative sequence is injected into the power grid. To solve this problem, RPC can be employed. In the following, the process of determining the compensating reference currents for the RPC is explained.

To make active currents of two sections balanced, the RPC can shift active power from light-loaded section to the heavy-loaded section. To achieve this goal, the transferred current should be half of the difference between load currents, that is, $\Delta I = (I_{Laa} - I_{Lba})/2$. As a result, three-phase currents can be written as

$$\begin{cases} \vec{i}'_a = \vec{i}_a - \Delta I = \frac{(I_{Laa} + I_{Lba})}{2} e^{-j(\pi/6)} \\ \vec{i}'_b = \vec{i}_b + \Delta I = \frac{(I_{Laa} + I_{Lba})}{2} e^{-j(\pi/2)} \\ \vec{i}'_c = -(\vec{i}'_a + \vec{i}'_b) = \frac{\sqrt{3}(I_{Laa} + I_{Lba})}{2} e^{j(2\pi/3)} \end{cases} \quad (6)$$

Now, to balance the three-phase currents and make them in phase with the corresponding phase voltages, a certain amount of reactive current must be added to phase a and phase b . With

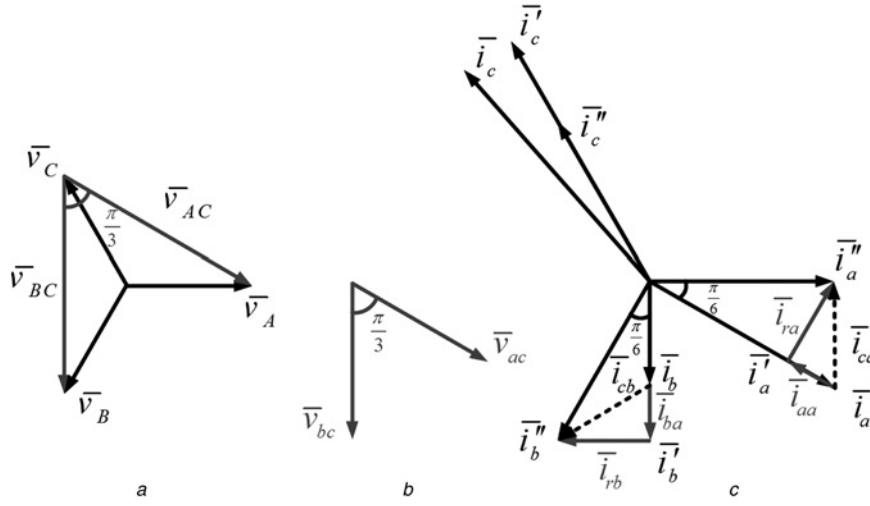


Fig. 2 Vector diagram

a Power grid voltages
b Feeder line-to-line voltages and
c Compensating currents

reference to Fig. 2c, the compensating reactive current should be

$$\begin{cases} \bar{i}_{ra} = \frac{(I_{Laa} + I_{Lba})}{2} \tan\left(\frac{\pi}{6}\right) e^{j(\pi/3)} \\ \bar{i}_{rb} = \frac{(I_{Laa} + I_{Lba})}{2} \tan\left(\frac{\pi}{6}\right) e^{-j\pi} \end{cases} \quad (7)$$

Hence, the phase currents of the secondary side of the transformer in balanced condition will be

$$\begin{cases} \bar{i}'_a = \bar{i}_a + \bar{i}_{ra} = \frac{\sqrt{3}(I_{Laa} + I_{Lba})}{3} e^{j0} \\ \bar{i}'_b = \bar{i}_b + \bar{i}_{rb} = \frac{\sqrt{3}(I_{Laa} + I_{Lba})}{3} e^{-j(2\pi/3)} \\ \bar{i}'_c = -(\bar{i}'_a + \bar{i}'_b) = \frac{\sqrt{3}(I_{Laa} + I_{Lba})}{3} e^{j(2\pi/3)} \end{cases} \quad (8)$$

As a result, the compensating reference currents of the RPC can be expressed as

$$\begin{cases} i_{ca} = i''_a - i_{La} \\ i_{cb} = i''_b - i_{Lb} \end{cases} \quad (9)$$

2.3 Control scheme

The control scheme proposed in [16] is represented in Fig. 3a. Considering (9), the first step to find the compensating currents is to detect the amplitude of currents of (8). Assume that the instantaneous currents of two loads are

$$\begin{cases} i_{La} = \sqrt{2}I_{La} \sin\left(\omega t - \frac{\pi}{6}\right) + \sqrt{2}I_{Lar} \sin\left(\omega t - \frac{2\pi}{3}\right) \\ + \sum_{h=2}^{\infty} \sqrt{2}I_{Lah} \sin(h\omega t + \varphi_{ah}) \\ i_{Lb} = \sqrt{2}I_{Lba} \sin\left(\omega t - \frac{\pi}{2}\right) + \sqrt{2}I_{Lbr} \sin(\omega t - \pi) \\ + \sum_{h=2}^{\infty} \sqrt{2}I_{Lbh} \sin(h\omega t + \varphi_{bh}) \end{cases} \quad (10)$$

then, based on the detection technique presented in [16], if i_{La} and i_{Lb} are multiplied by signals $\sin(\omega t - \pi/6)$ and $\sin(\omega t - \pi/2)$, respectively,

it gives

$$\begin{cases} i_{La} \times \sin\left(\omega t - \frac{\pi}{6}\right) = \frac{\sqrt{2}}{2}I_{La} - \frac{\sqrt{2}}{2}I_{La} \cos\left(2\omega t - \frac{\pi}{3}\right) \\ - \frac{\sqrt{2}}{2}I_{Lar} \cos\left(2\omega t - \frac{5\pi}{6}\right) + \sum_{h=2}^{\infty} \sqrt{2}I_{Lah} \sin(h\omega t + \varphi_{ah}) \sin\left(\omega t - \frac{\pi}{6}\right) \\ i_{Lb} \times \sin\left(\omega t - \frac{\pi}{2}\right) = \frac{\sqrt{2}}{2}I_{Lb} - \frac{\sqrt{2}}{2}I_{Lb} \cos(2\omega t - \pi) \\ - \frac{\sqrt{2}}{2}I_{Lbr} \cos\left(2\omega t - \frac{3\pi}{2}\right) + \sum_{h=2}^{\infty} \sqrt{2}I_{Lbh} \sin(h\omega t + \varphi_{bh}) \sin\left(\omega t - \frac{\pi}{2}\right) \end{cases} \quad (11)$$

Passing the sum of the obtained results through a LPF and then multiplying it by $2/\sqrt{3}$, the amplitude of i''_a and i''_b will be obtained. The balanced currents can then be achieved through multiplying the amplitude of i''_a and i''_b by $\sin(\omega t)$ and $\sin(\omega t - 2\pi/3)$, respectively.

To achieve the desired operation of the RPC, a stable DC-link voltage is necessary. The capacitor should absorb or release energy when its voltage is below or above the reference value, respectively. This goal is achieved in [16] by using a PI controller. The controller output is multiplied with the synchronous voltage signals and then is added to the corresponding reference currents of phase a and phase b . Finally, the compensating reference currents can be fed to the RPC current controllers.

3 Improved control strategy

The aforementioned control strategy for the RPC can be regarded as the basic method for detection and realising the compensating reference currents. In the following, some modifications are proposed to enhance the performance of the control scheme in terms of dynamic response and tracking performance. The improved control strategy is illustrated in Fig. 3b, and different contributions, highlighted in the figure, are explained in the following sections.

3.1 Active current fundamental component detection

A cursory examination of (11) reveals that after multiplying the load currents with corresponding synchronous signals, a second-order

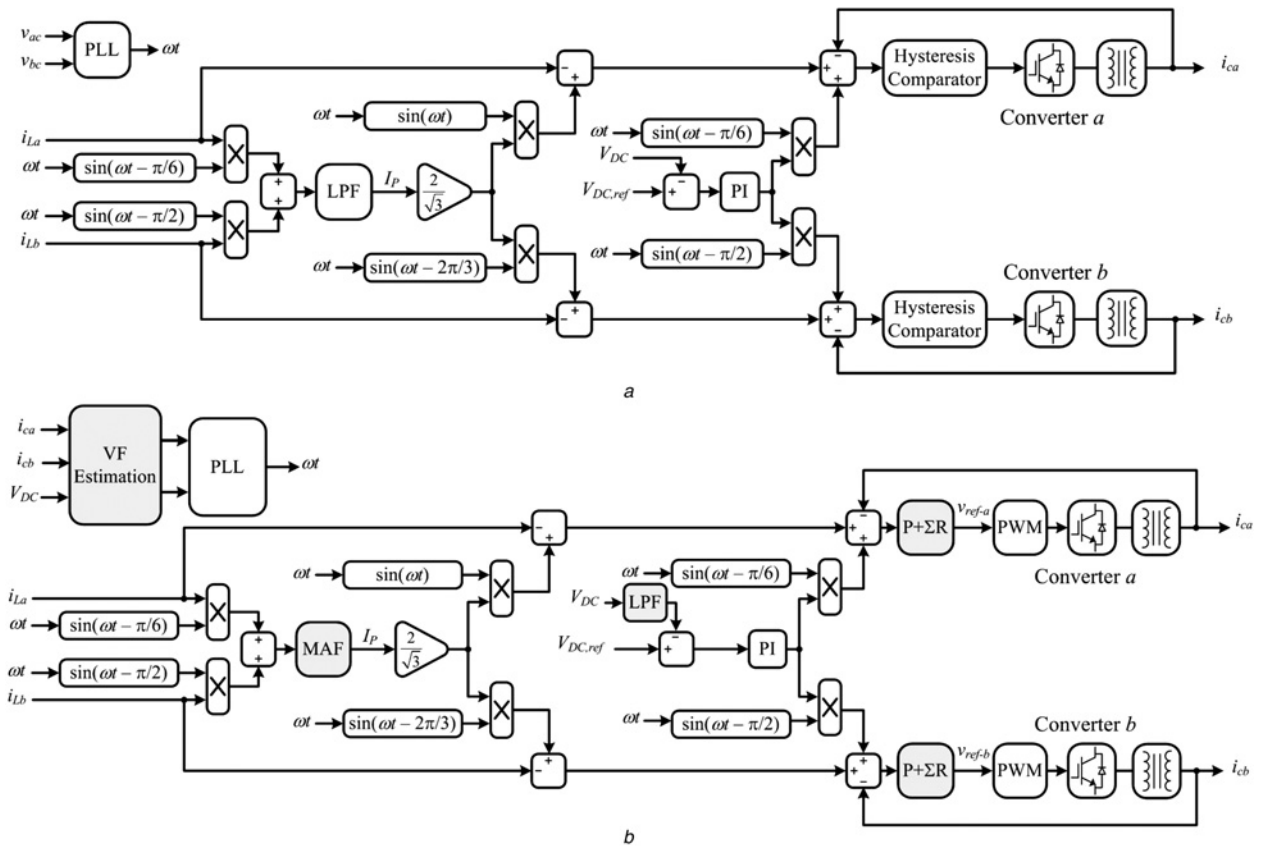


Fig. 3 Control strategy of RPC converter

a Conventional method [16]

b Improved method

harmonic component with an amplitude as high as the DC component has appeared. Thus, the elimination of these low frequency and high-amplitude components requires the use of a first- or a second-order LPF with a very low cut-off frequency or a high-order LPF. In addition to stability problems, a high-order LPF imposes high computational burden [19, 26]. By contrast, using a low-order LPF with a low cut-off frequency significantly degrades the transient performance of the system. To meet this challenge, adopting a MAF can be recommended instead of the conventional LPFs.

A MAF is a linear-phase finite-impulse-response filter which can be considered as an ideal LPF [20]. Simple practical implementation and low computational burden can be counted as its main advantages.

Continuous-time domain description of MAF, where $x(t)$ is the input signal and $\bar{x}(t)$ is the output signal, is

$$\bar{x}(t) = \frac{1}{T_w} \int_{t-T_w}^t x(\tau) d\tau \quad (12)$$

in which T_w indicates the filtering window length. From (12), the MAF transfer function can be derived as

$$G_{\text{MAF}}(s) = \frac{\bar{x}(s)}{x(s)} = \frac{1 - e^{-T_w s}}{T_w s} \quad (13)$$

As (13) reveals, the MAF requires a time equal to its window length to reach the steady-state condition. It denotes that the transient response will be degraded when the filtering window becomes wider. In addition, MAF provides unity gain for DC component and at frequencies $f = n/T_w$ ($n = 1, 2, 3, \dots$) the gain is zero. Regarding our application, owing to the existence of double frequency components in the input signal to the filter, $T_w = 1/100$ s is an appropriate selection. Fig. 4 shows the Bode plots of MAF compared with a LPF with the same cut-off frequency.

Apparently, the MAF provides high attenuation at all harmonic currents starting from the second-order one. This unique feature improves the filtering performance while the filter bandwidth and transient performance are not alleviated.

Assuming that the window length of the MAF contains N samples of its input signal, that is, $T_w = NT_s$, where T_s is the sampling time, the discrete-time description of MAF can be concluded as

$$\bar{x}(k) = \frac{1}{N} \sum_{i=0}^{N-1} x(k-i) \quad (14)$$

where $x(k)$ is the current sample.

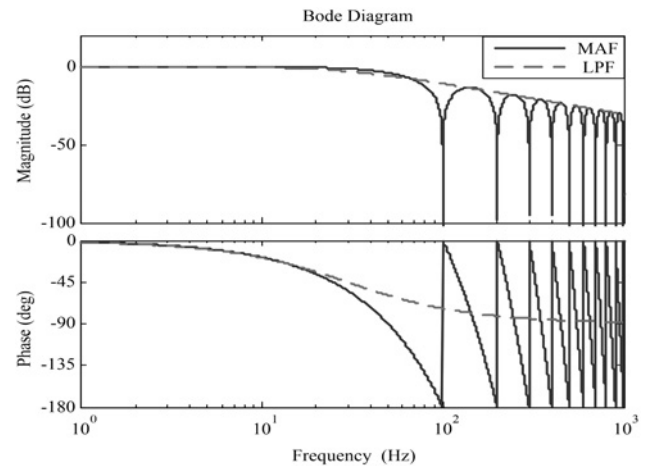


Fig. 4 Bode diagram of MAF and its first-order LPF counterpart for $T_w = 0.01$ s

The difference (14) can be written in Z-domain as

$$\bar{X}(z) = G_{\text{MAF}}(z)X(z) = \frac{1}{N} \frac{1 - z^{-N}}{1 - z^{-1}} X(z) \quad (15)$$

Fig. 5 depicts the discrete-time realisation of the MAF based on (15).

3.2 Outer DC-link voltage loop

The rule of this loop is to regulate the voltage of DC-link to a reference signal using a simple PI compensator. Transfer function of the PI controller can be expressed as

$$G_{\text{PI}} = K_{\text{pv}} + \frac{K_{\text{iv}}}{s} \quad (16)$$

where K_{pv} and K_{iv} are proportional and integral gains, respectively. The output of PI compensator, which is dependent to the exchanged power, presents a ripple at twice the grid frequency [21]. To attenuate this undesirable ripple, a LPF with a cut-off frequency lower than twice the grid frequency is proposed.

3.3 Inner current control loop

To enhance the tracking performance of inner current loop and also, provide the possibility of using a PWM modulator such as a sinusoidal PWM, a current controller must be employed. A PR controller is adopted in this paper to assure near-zero error at the steady-state. Theoretically, a PR controller is able to eliminate the steady-state error of a sinusoidal signal with the same frequency as its resonance frequency [22–24]. Due to the multi-harmonic nature of the compensating currents, several resonant blocks tuned at desired harmonic frequencies are needed. The transfer function of a cascading PR controller can be defined as

$$G_{\text{PR}} = K_p + \sum_{h \in N} \frac{2K_i \omega_c s}{s^2 + 2\omega_c s + (h\omega)^2} \quad (17)$$

In this equation, K_p is the proportional gain, h represents the harmonic order to be omitted, N is a set of harmonics and K_i denotes the individual resonant gain. Moreover, ω is the fundamental frequency and ω_c determines the bandwidth of each resonant block.

To specify the PR parameters, a model of the system is of great importance. The transfer function of each single phase converter can be written as follows

$$G_{\text{conv}} = \frac{i_c}{v_{\text{conv}}} = \frac{1}{K_s} \frac{e^{-T_d s}}{Ls + R} \quad (18)$$

in which, L and R denote the inductance and the resistance of the filter inductor, respectively and T_d indicates the delay introduced by digital sampling, algorithm computation time and PWM modulation. Fig. 6 shows the Bode diagram of converter in presence of cascading PR controller with $N = \{1, 5, 7, 11, 13\}$ and parameters of Table 1.

With respect to Fig. 6, owing to the intense phase variations at resonance frequency of PR controllers, the gain crossover frequency, ω_{cr} , should be chosen higher than these frequencies to assure a suitable phase margin (PM). Assuming ω_{cr} is so higher than the resonance frequency, the influence of resonant block can

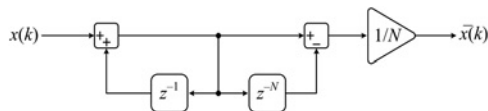


Fig. 5 Discrete-time implementation of MAF

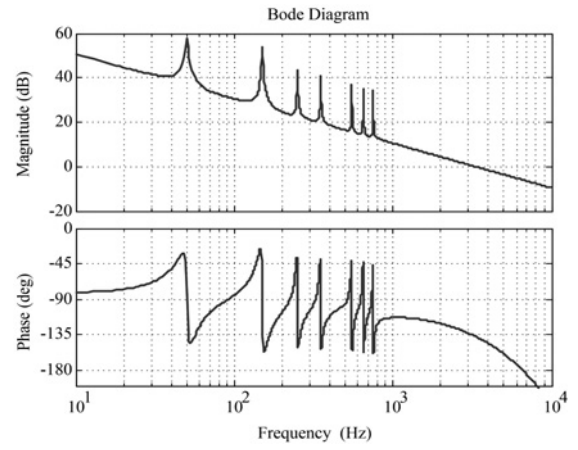


Fig. 6 Bode diagram of PR controller

be neglected at this frequency; consequently, the effect of resonant blocks can be ignored in stability analysis based design. Therefore, the proportional gain of controller can be obtained as

$$K_p = \frac{1}{|G_{\text{conv}}(j\omega_{\text{cr}})|} \simeq K_s \omega_{\text{cr}} L \quad (19)$$

Designing a controller with proper PM ($\pi/4 < \text{PM} < \pi/3$) recommends a gain crossover frequency (ω_{cr}) lower than $\omega_{\text{sw}}/6$, where ω_{sw} is the switching frequency.

4 Voltage sensorless synchronisation based on VF

According to the aforementioned description, three kind of sensors (DC voltage, AC voltages and AC currents) are required for normal operation of the control strategy. A DC voltage sensor is required for maintaining the DC-link voltage at its rated value. Two AC voltage sensors are utilised to detect the phase angle of the grid voltage to generate balanced reference currents. Four AC current sensors are also needed for current control loops and for finding the reference compensating currents. This number of sensors increases the volume and the cost of the system. While DC-link voltage and AC current sensors are necessarily required for over/under voltage and overcurrent protection purposes, respectively, the grid voltage sensors are only needed for synchronisation purpose and may be readily replaced by some kind of software estimation algorithm. Although numerous works have been presented in an attempt to eliminate grid voltage sensors in the application of grid-connected converters, no similar study has been carried out for RPC systems, to the best knowledge of authors.

4.1 Virtual flux estimation for grid synchronisation

The VF estimation is premised on the definition of flux, ψ , and can be formulated as

$$\psi = \int v dt + \psi_0 \quad (20)$$

where ψ_0 is referred to as the initial value of ψ . Taking into account the system configuration of Fig. 1 and from writing the KVL

Table 1 Controllers parameters

Parameter	K_{pv}	K_{iv}	ω_{cr}	K_p	K_i	ω_c
value	0.18	2.9	6600π	288	3000	5

Table 2 Traction power system and RPC parameters

Parameter	Value
grid side line voltage (root-mean-square [RMS])	220 kV
grid frequency	50 Hz
K_T	220/27.5
K_S	27.5/1
switching frequency	20 kHz
L_a, L_b	0.5 mH
DC-link capacitor	40 mF

equation for the output of RPC and secondary side of the step-down transformer, it gives

$$v' = v_{\text{conv}} - Ri'_c - L \frac{di'_c}{dt} \quad (21)$$

In this equation, v' is the secondary side voltage of the step-down transformer, v_{conv} represents the output voltage of the converter and i'_c is the converter current. Combining (20) and (21), and considering in PWM operation v_{conv} can be equal with reference voltage of the converter, the VF can be calculated as

$$\psi = \int (v_{\text{ref}} - Ri'_c) dt - Li'_c \quad (22)$$

In this equation, v_{ref} is the reference voltage of the converter. Moreover, the initial value of flux is needed for the estimation but it will be ignored in the following analysis.

According to (22), the estimation of VF that is based on ideal integration is susceptible to drift and saturation of the estimated values. Hence, the integral part usually is implemented by digital filters in practice. The simplest estimation techniques are usually based on low-pass or band-pass filters that are tuned to emulate integration for the grid voltage fundamental frequency. However, these approaches have small errors in the amplitude or phase angle

of the estimated VF. Numerous filters have been proposed that can deal with this problem effectively [25]. However, with respect to the harmonic nature of the compensation currents, a filter should be adopted which can reduce the effect of the frequencies higher than fundamental frequency.

4.2 Second-order LPF virtual flux estimation

A second-order LPF passes the fundamental frequency with unity gain and $\pi/2$ rad phase shift and also, degrades the effect of other harmonics. The transfer function of the filter from the input variable, v , to the filtered variable, v' , is given by

$$\frac{v'(s)}{v(s)} = \frac{k\omega}{s^2 + k\omega s + \omega^2} \quad (23)$$

where ω is the grid angular frequency. As it is obvious, the gain k determines the shape of frequency response. For a good trade-off between transient and steady state characteristics, the value of k is chosen equal to $\sqrt{2}$ in this study.

Since the VF is equivalent with the integral of the voltage, the voltage phase angle, θ_f , can be calculated by leading the instantaneous phase angle of the flux, γ_f , by $\pi/2$, that is

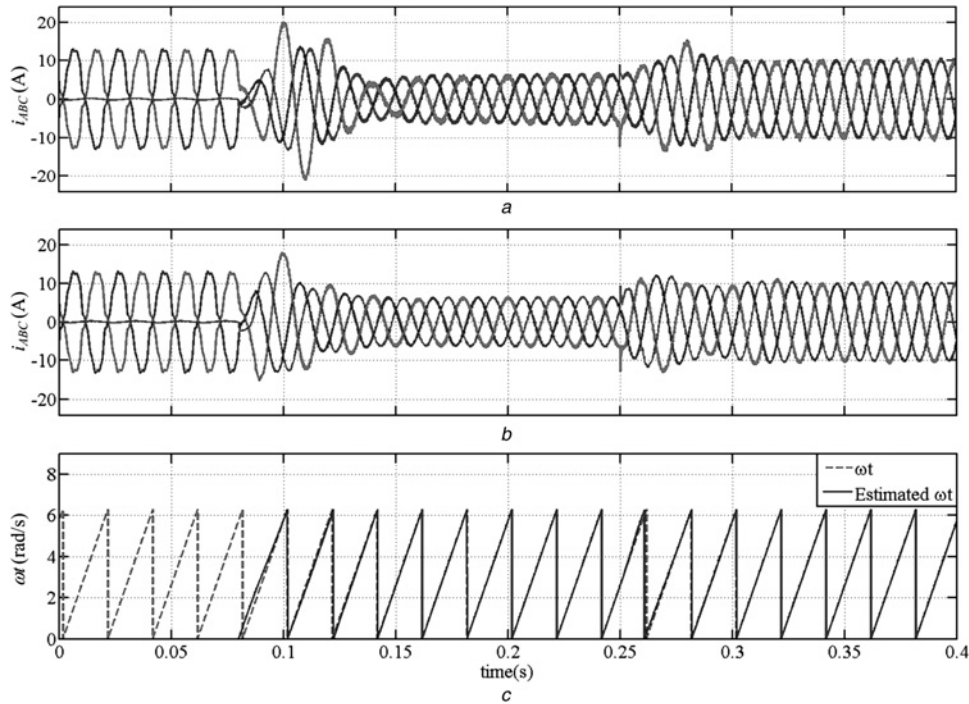
$$\theta_f = \gamma_f + \frac{\pi}{2} \quad (24)$$

In this equation, γ_f can be calculated using the estimated flux of two feeder sections and then, feeding them into a phase-locked loop.

Using the proposed sensorless method, (22) can be rewritten for the RPC as follows

$$\begin{cases} \psi_{ac} = \int (v_{\text{ref}-a} - R_a i'_{ca}) dt - L_a i'_{ca} \\ \psi_{bc} = \int (v_{\text{ref}-b} - R_b i'_{cb}) dt - L_b i'_{cb} \end{cases} \quad (25)$$

where i'_{ca} and i'_{cb} are the currents of the secondary side of the step-down transformers a and b , respectively.

**Fig. 7** Simulation results

- a Grid three-phase currents by using conventional control strategy
- b Grid three-phase currents by using improved sensorless control strategy
- c Comparison of measured and estimated phase of grid voltage

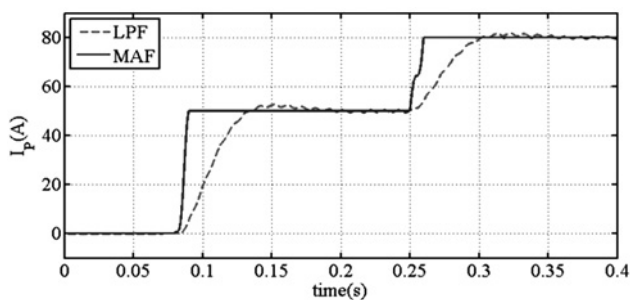
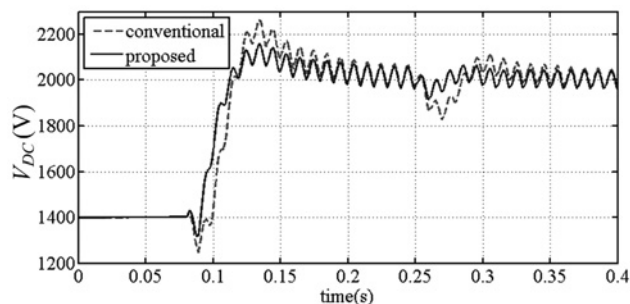
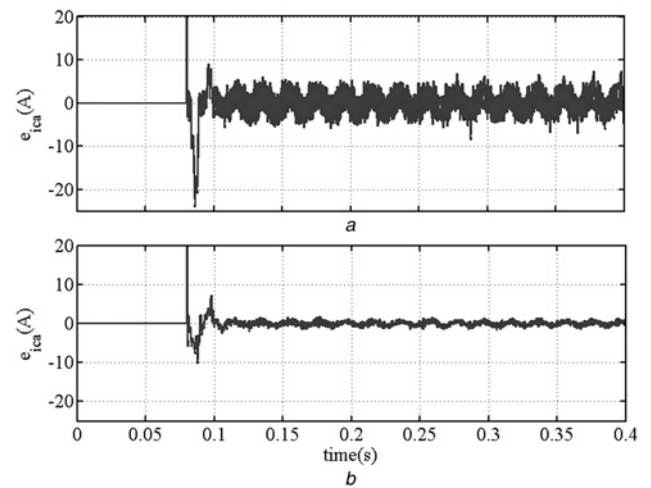
Table 3 Grid current characteristics before and after compensation

Case	I_a		I_b		I_c	
	RMS, A	THD, %	RMS, A	THD, %	RMS, A	THD, %
before compensation	8.89	11.16	0.14	3.60	8.79	11.29
conventional method	4.43	2.48	4.48	2.22	4.42	3.75
improved method	4.45	1.01	4.47	1.12	4.50	1.61

5 Performance evaluation

To validate the superior performance of the improved sensorless control strategy in comparison with the conventional one, already reported in [16], both techniques are simulated in Matlab/Simulink. The high-speed railway electric locomotives are considered as a linear resistive load and harmonic current source with the power factor close to one. System parameters are listed in Table 2. The effect of delays originated from digital sampling, algorithm computation time and PWM modulation is considered in simulations. A PR controller including six resonant blocks is used (tuned at 1st, 3rd, 5th, 7th, 11th and 13th harmonics). The parameters of the controllers and filters of the improved strategy are listed in Table 1. As evident from Fig. 3a, the conventional strategy uses hysteresis current controllers in its structure. Consequently, to attain an acceptable level of current harmonics, larger inductances (1 mH) are used as RPC filters in the conventional control strategy, which are twice those of the proposed technique. Furthermore, voltage sensors are used to detect the grid phase angle in the conventional method, while the improved method utilises the proposed sensorless technique. Moreover, the bandwidth of LPFs, used in the detection part of the conventional method, is chosen as 10 Hz and other parameters of two methods are the same.

The simulation test is carried out under the situation that the locomotive *a* and the locomotive *b* draw currents with the fundamental amplitude of 100 and 60 A, respectively, and the THD is 11%. Figs. 7a and b shows the grid current waveforms before

**Fig. 8** Detection of sum of two DC components**Fig. 9** Comparison of DC-link voltage for two methods**Fig. 10** Error of compensating current of section *a* for
a Hysteresis method
b PR method

and after compensation for two compensation strategies. First, only section *a* is loaded and the RPC system is off. As it is obvious, the train system injects a considerable amount of negative sequence and harmonic components into the power grid. The RPC switches on at 0.08 s. After compensation, the power grid currents become almost balanced and the harmonic contents are significantly reduced. Table 3 compares grid current characteristics before and after compensation when only load *a* is connected for two methods. THD values are calculated up to 50th order harmonics. Cursory examination of the results reveals that the proposed method exhibits a better performance than the conventional method in providing balanced and sinusoidal currents. Moreover, the CUF reaches acceptable value of 1% for two methods.

To confirm the robustness and superior dynamic performance of the proposed method, the load *b* is connected at $t=0.25$ s. As it is obvious, although a sensorless method is adopted to estimate grid frequency angle, the improved control strategy can rapidly reach the steady-state. Fig. 7c compares the phase of grid voltage obtained from measured and sensorless method. As the result reveals, the estimated phase can rapidly and accurately follow the obtained phase from the measured voltages. This appropriate behaviour can be attributed to the use of MAF instead of LPF to generate I_p in the improved method. Fig. 8 shows the output of MAF and LPF in the proposed and conventional methods, respectively. The transient and steady-state response of MAF is better than LPF, which it entails improving the quality of the compensated currents and fast response of the system. Fig. 9 depicts the voltage of DC-link for two methods. The influence of using LPF and the speed of the system can be seen on the variation of DC-link voltage. The input of hysteresis comparator and PR controller are shown in Fig. 10. The figure shows that the PR controllers can effectively eliminate the steady-state error.

6 Conclusions

An improved grid voltage sensorless method for control of the RPC has been proposed in this paper. The control strategy has been improved in several aspects. A MAF has been added to enhance the speed and accuracy of the detection method. A LPF has been applied to the DC-link control loop. Furthermore, a PR controller has been used to improve the tracking performance of the reference currents. In another part of the paper, a sensorless VF method has been presented for eliminating AC voltage sensors. Simulation results have demonstrated the effectiveness of the proposed method.

7 References

- 1 Dai, N.Y., Ch Wong, M., Lao, K.W., *et al.*: 'Modelling and control of a railway power conditioner in co-phase traction power system under partial compensation', *IET Power Electron.*, 2014, **7**, (5), pp. 1044–1054
- 2 Dai, N.Y., Lao, K.W., Wong, M.C., *et al.*: 'Hybrid power quality conditioner for co-phase power supply system in electrified railway', *IET Power Electron.*, 2012, **5**, (7), pp. 1084–1094
- 3 Ma, F., Luo, A., Xu, X., *et al.*: 'A simplified power conditioner based on half-bridge converter for high-speed railway system', *IEEE Trans. Ind. Electron.*, 2013, **60**, (2), pp. 728–738
- 4 Wang, B., Dong, X.Z., Bo, Z.Q., *et al.*: 'Negative-sequence pilot protection with applications in open-phase transmission lines', *IEEE Trans. Power Deliv.*, 2010, **25**, (3), pp. 1306–1313
- 5 De, D., Ramanarayanan, V.: 'Decentralized parallel operation of inverters sharing unbalanced and nonlinear loads', *IEEE Trans. Power Electron.*, 2010, **25**, (12), pp. 3015–3025
- 6 Tenti, P., Costabeber, A., Mattavelli, P., *et al.*: 'Distribution loss minimization by token ring control of power electronic interfaces in residential microgrids', *IEEE Trans. Ind. Electron.*, 2012, **59**, (10), pp. 3817–3826
- 7 Zhang, Z.W., Wu, B., Kang, J.S., *et al.*: 'A multi-purpose balanced transformer for railway traction applications', *IEEE Trans. Power Deliv.*, 2009, **24**, (2), pp. 711–718
- 8 Bueno, A., Aller, J.M., Restrepo, J., *et al.*: 'Harmonic and balance compensation using instantaneous active and reactive power control on electric railway systems'. Proc. Appl. Power Electron. Conf. Expo., 2010, pp. 1139–1144
- 9 Hu, L., Morrison, R.: 'Reduction of harmonic distortion and improvement of voltage form factor in a compensated railway system with a single arm filter'. IEEE Conf. Harmonics in Power Systems (ICHIPSS), 1992, pp. 1433–1439
- 10 Jianzong, M., Mingli, W., Shaobing, Y.: 'The application of SVC for the power quality control of electric railways'. Proc. Int. Conf. Sustainable Power Generation Supply, 2009, pp. 1–4
- 11 Guiping, Z., Jianye, C., Xiaoyu, L.: 'Compensation for the negative-sequence currents of electric railway based on SVC'. Proc. Third IEEE Conf. Ind. Electronics Applications, 2008, pp. 1958–1963
- 12 Wu, Ch., Luo, A., Shen, J., *et al.*: 'A negative sequence compensation method based on a two-phase three-wire converter for a high-speed railway traction power supply system', *IEEE Trans. Power Electron.*, 2012, **27**, (2), pp. 706–717
- 13 Sun, Z., Jiang, X., Zhu, D., *et al.*: 'A novel active power quality compensator topology for electrified railway', *IEEE Trans. Power Electron.*, 2004, **19**, (4), pp. 1036–1042
- 14 Lao, K.-W., Dai, N., Liu, W.-G., *et al.*: 'Hybrid power quality compensator with minimum DC operation voltage design for high-speed traction power systems', *IEEE Trans. Power Electron.*, 2013, **28**, (4), pp. 2024–2036
- 15 Luo, A., Ma, F., Wu, C., *et al.*: 'A dual-loop control strategy of railway static power regulator under V/V electric traction system', *IEEE Trans. Power Electron.*, 2011, **26**, (7), pp. 2079–2091
- 16 Luo, A., Wu, Ch., Shen, J., *et al.*: 'Railway static power conditioners for high-speed train traction power supply systems using three-phase V/V transformers', *IEEE Trans. Power Electron.*, 2011, **26**, (10), pp. 2844–2856
- 17 Ahmed, K.H., Massoud, A.M., Finney, S.J., *et al.*: 'Autonomous adaptive sensorless controller of inverter-based islanded-distributed generation system', *IET Power Electronics*, 2009, **2**, (3), pp. 256–266
- 18 Gonzalez Norniella, J., Cano, J.M., Orcajo, G.A., *et al.*: 'Improving the dynamics of virtual-flux-based control of three-phase active rectifiers', *IEEE Trans. Ind. Electron.*, 2014, **61**, (1), pp. 177–187
- 19 Liu, T., Xia, Ch., Shi, T.: 'Robust model predictive current control of grid-connected converter without alternating current voltage sensors', *IET Power Electron.*, 2014, **7**, (12), pp. 2934–2944
- 20 Golestan, S., Ramezani, M., Guerrero, J.M., *et al.*: 'Moving average filter based phase-locked loops: performance analysis and design guidelines', *IEEE Trans. Power Electron.*, 2014, **29**, (6), pp. 2750–2763
- 21 Miret, J., Castilla, M., Matas, J., *et al.*: 'Selective harmonic-compensation control for single-phase active power filter with high harmonic rejection', *IEEE Trans. Ind. Electron.*, 2009, **56**, (8), pp. 3117–3127
- 22 Zmood, D.N., Holmes, D.G.: 'Stationary frame current regulation of PWM inverters with zero steady-state error', *IEEE Trans. Power Electron.*, 2003, **18**, (3), pp. 814–822
- 23 Vidal, A., Freijedo, F.D., Yepes, A.G., *et al.*: 'Transient response evaluation of stationary-frame resonant current controllers for grid-connected applications', *IET Power Electron.*, 2014, **7**, (7), pp. 1714–1724
- 24 Li, B., Yao, W., Hang, L., *et al.*: 'Robust proportional resonant regulator for grid-connected voltage source inverter (VSI) using direct pole placement design method', *IET Power Electron.*, 2012, **5**, (8), pp. 1367–1373
- 25 Suul, J.A., Luna, A., Rodriguez, P., *et al.*: 'Voltage sensor-less synchronization to unbalanced grids by frequency-adaptive virtual flux estimation', *IEEE Trans. Ind. Electron.*, 2012, **59**, (7), pp. 2910–2923
- 26 Monfared, M., Golestan, S., Guerrero, J.M.: 'A new synchronous reference frame-based method for single-phase shunt active power filters', *J. Power Electron.*, 2013, **13**, (4), pp. 692–700